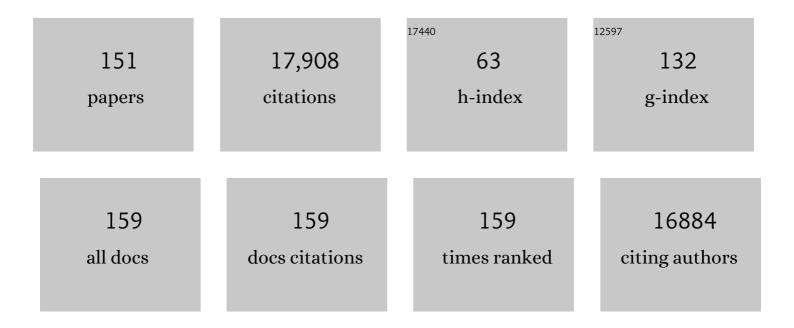
David Mitlin

List of Publications by Year in descending order

Source: https://exaly.com/author-pdf/6011449/publications.pdf Version: 2024-02-01



ΠΛΛΙΠ ΜΙΤΙΙΝ

#	Article	IF	CITATIONS
1	A Sodium–Antimony–Telluride Intermetallic Allows Sodiumâ€Metal Cycling at 100% Depth of Discharge and as an Anodeâ€Free Metal Battery. Advanced Materials, 2022, 34, e2106005.	21.0	40
2	Multifunctional Separator Allows Stable Cycling of Potassium Metal Anodes and of Potassium Metal Batteries. Advanced Materials, 2022, 34, e2105855.	21.0	45
3	Multifunctional Separator Allows Stable Cycling of Potassium Metal Anodes and of Potassium Metal Batteries (Adv. Mater. 7/2022). Advanced Materials, 2022, 34, .	21.0	1
4	Review of Multifunctional Separators: Stabilizing the Cathode and the Anode for Alkali (Li, Na, and K) Metal–Sulfur and Selenium Batteries. Chemical Reviews, 2022, 122, 8053-8125.	47.7	132
5	Review of modification strategies in emerging inorganic solid-state electrolytes for lithium, sodium, and potassium batteries. Joule, 2022, 6, 543-587.	24.0	90
6	Molybdenum Carbide Electrocatalyst In Situ Embedded in Porous Nitrogenâ€Rich Carbon Nanotubes Promotes Rapid Kinetics in Sodiumâ€Metal–Sulfur Batteries. Advanced Materials, 2022, 34, e2106572.	21.0	33
7	Revealing the Solidâ€State Electrolyte Interfacial Stability Model with Na–K Liquid Alloy. Angewandte Chemie - International Edition, 2022, 61, .	13.8	10
8	Thermally fabricated cobalt telluride in nitrogen-rich carbon dodecahedra as high-rate potassium and sodium ion battery anodes. Sustainable Energy and Fuels, 2022, 6, 3582-3590.	4.9	9
9	Sulfur and nitrogen codoped cyanoethyl celluloseâ€derived carbon with superior gravimetric and volumetric capacity for potassium ion storage. , 2022, 4, 986-1001.		36
10	Phase Engineering of Defective Copper Selenide toward Robust Lithium–Sulfur Batteries. ACS Nano, 2022, 16, 11102-11114.	14.6	50
11	Lithium-activated SnS–graphene alternating nanolayers enable dendrite-free cycling of thin sodium metal anodes in carbonate electrolyte. Energy and Environmental Science, 2021, 14, 382-395.	30.8	65
12	Emerging trends in anion storage materials for the capacitive and hybrid energy storage and beyond. Chemical Society Reviews, 2021, 50, 6734-6789.	38.1	93
13	Understanding the Strength of the Selenium–Graphene Interfaces for Energy Storage Systems. Langmuir, 2021, 37, 2029-2039.	3.5	11
14	Heavily Tungstenâ€Đoped Sodium Thioantimonate Solid‣tate Electrolytes with Exceptionally Low Activation Energy for Ionic Diffusion. Angewandte Chemie, 2021, 133, 26362-26370.	2.0	2
15	Heavily Tungstenâ€Ðoped Sodium Thioantimonate Solidâ€State Electrolytes with Exceptionally Low Activation Energy for Ionic Diffusion. Angewandte Chemie - International Edition, 2021, 60, 26158-26166.	13.8	18
16	Selenium infiltrated hierarchical hollow carbon spheres display rapid kinetics and extended cycling as lithium metal battery (LMB) cathodes. Journal of Materials Chemistry A, 2021, 9, 18582-18593.	10.3	5
17	Alloying of Alkali Metals with Tellurene. Advanced Energy Materials, 2021, 11, 2003248.	19.5	11
18	Sulfur-Rich Graphene Nanoboxes with Ultra-High Potassiation Capacity at Fast Charge: Storage Mechanisms and Device Performance. ACS Nano, 2021, 15, 1652-1665.	14.6	132

#	Article	IF	CITATIONS
19	Dendriteâ€Free Potassium Metal Anodes in a Carbonate Electrolyte. Advanced Materials, 2020, 32, e1906735.	21.0	107
20	Site-Specific Sodiation Mechanisms of Selenium in Microporous Carbon Host. Nano Letters, 2020, 20, 918-928.	9.1	30
21	Review of Emerging Concepts in SEI Analysis and Artificial SEI Membranes for Lithium, Sodium, and Potassium Metal Battery Anodes. Advanced Energy Materials, 2020, 10, 2002297.	19.5	292
22	Biomimetic composite architecture achieves ultrahigh rate capability and cycling life of sodium ion battery cathodes. Applied Physics Reviews, 2020, 7, .	11.3	15
23	Potassium Metal Batteries: Stable Potassium Metal Anodes with an Allâ€Aluminum Current Collector through Improved Electrolyte Wetting (Adv. Mater. 49/2020). Advanced Materials, 2020, 32, 2070365.	21.0	1
24	Stable Lithium Sulfur Battery Based on In Situ Electrocatalytically Formed Li ₂ S on Metallic MoS ₂ –Carbon Cloth Support. Small Methods, 2020, 4, 2000353.	8.6	49
25	Dry and Wet CO 2 Capture from Milkâ€Derived Microporous Carbons with Tuned Hydrophobicity. Advanced Sustainable Systems, 2020, 4, 2000001.	5.3	3
26	Stable Potassium Metal Anodes with an Allâ€Aluminum Current Collector through Improved Electrolyte Wetting. Advanced Materials, 2020, 32, e2002908.	21.0	70
27	Cobalt phosphide (Co ₂ P) encapsulated in nitrogen-rich hollow carbon nanocages with fast rate potassium ion storage. Chemical Communications, 2020, 56, 14889-14892.	4.1	25
28	Tutorial review on structure – dendrite growth relations in metal battery anode supports. Chemical Society Reviews, 2020, 49, 7284-7300.	38.1	130
29	Emerging Potassium Metal Anodes: Perspectives on Control of the Electrochemical Interfaces. Accounts of Chemical Research, 2020, 53, 1161-1175.	15.6	105
30	Graphene-like Vanadium Oxygen Hydrate (VOH) Nanosheets Intercalated and Exfoliated by Polyaniline (PANI) for Aqueous Zinc-Ion Batteries (ZIBs). ACS Applied Materials & Interfaces, 2020, 12, 31564-31574.	8.0	126
31	Potassium Batteries: Dendriteâ€Free Potassium Metal Anodes in a Carbonate Electrolyte (Adv. Mater.) Tj ETQq1 3	1 0.78431 21.0	4 rgBT /Ove
32	High Capacity Adsorption—Dominated Potassium and Sodium Ion Storage in Activated Crumpled Graphene. Advanced Energy Materials, 2020, 10, 1903280.	19.5	72
33	Sulfur-nitrogen rich carbon as stable high capacity potassium ion battery anode: Performance and storage mechanisms. Energy Storage Materials, 2020, 27, 212-225.	18.0	235
34	Review of Emerging Potassium–Sulfur Batteries. Advanced Materials, 2020, 32, e1908007.	21.0	91
35	First Atomic-Scale Insight into Degradation in Lithium Iron Phosphate Cathodes by Transmission Electron Microscopy. Journal of Physical Chemistry Letters, 2020, 11, 4608-4617.	4.6	16
36	A functional SrF ₂ coated separator enabling a robust and dendrite-free solid electrolyte interphase on a lithium metal anode. Journal of Materials Chemistry A, 2019, 7, 21349-21361.	10.3	47

#	Article	IF	CITATIONS
37	Potassiumâ€lon Batteries: Sulfurâ€Grafted Hollow Carbon Spheres for Potassiumâ€lon Battery Anodes (Adv.) Tj E	101 1 0.7	784314 rgt
38	Potassium Ion Storage: Direct Structure–Performance Comparison of All arbon Potassium and Sodium Ion Capacitors (Adv. Sci. 12/2019). Advanced Science, 2019, 6, 1970075.	11.2	3
39	Synergy of Epoxy Chemical Tethers and Defectâ€Free Graphene in Enabling Stable Lithium Cycling of Silicon Nanoparticles. Angewandte Chemie, 2019, 131, 16743-16753.	2.0	8
40	Synergy of Epoxy Chemical Tethers and Defectâ€Free Graphene in Enabling Stable Lithium Cycling of Silicon Nanoparticles. Angewandte Chemie - International Edition, 2019, 58, 16590-16600.	13.8	50
41	Sulfurâ€Grafted Hollow Carbon Spheres for Potassiumâ€ion Battery Anodes. Advanced Materials, 2019, 31, e1900429.	21.0	235
42	Direct Structure–Performance Comparison of All arbon Potassium and Sodium Ion Capacitors. Advanced Science, 2019, 6, 1802272.	11.2	98
43	Selenium-sulfur (SeS) fast charging cathode for sodium and lithium metal batteries. Energy Storage Materials, 2019, 20, 71-79.	18.0	50
44	Sodium Metal Anodes: Emerging Solutions to Dendrite Growth. Chemical Reviews, 2019, 119, 5416-5460.	47.7	572
45	Lithium Ion Capacitor with Identical Carbon Electrodes Yields 6 s Charging and 100â€ ⁻ 000 Cycles Stability with 1% Capacity Fade. ACS Sustainable Chemistry and Engineering, 2019, 7, 2867-2877.	6.7	38
46	Pristine or Highly Defective? Understanding the Role of Graphene Structure for Stable Lithium Metal Plating. Advanced Energy Materials, 2019, 9, 1802918.	19.5	99
47	Internal structure – Na storage mechanisms – Electrochemical performance relations in carbons. Progress in Materials Science, 2018, 97, 170-203.	32.8	100
48	Fundamental Insight into Zr Modification of Li- and Mn-Rich Cathodes: Combined Transmission Electron Microscopy and Electrochemical Impedance Spectroscopy Study. Chemistry of Materials, 2018, 30, 2566-2573.	6.7	106
49	Directional Flow-Aided Sonochemistry Yields Graphene with Tunable Defects to Provide Fundamental Insight on Sodium Metal Plating Behavior. ACS Nano, 2018, 12, 12255-12268.	14.6	48
50	Liâ€Rich Li[Li _{1/6} Fe _{1/6} Ni _{1/6} Mn _{1/2}]O ₂ (LFNMO) Cathodes: Atomic Scale Insight on the Mechanisms of Cycling Decay and of the Improvement due to Cobalt Phosphate Surface Modification. Small, 2018, 14, e1802570.	10.0	41
51	Review of Hybrid Ion Capacitors: From Aqueous to Lithium to Sodium. Chemical Reviews, 2018, 118, 6457-6498.	47.7	741
52	β-SnSb for Sodium Ion Battery Anodes: Phase Transformations Responsible for Enhanced Cycling Stability Revealed by In Situ TEM. ACS Energy Letters, 2018, 3, 1670-1676.	17.4	90
53	Selenium Impregnated Monolithic Carbons as Free‣tanding Cathodes for High Volumetric Energy Lithium and Sodium Metal Batteries. Advanced Energy Materials, 2018, 8, 1701918.	19.5	132
54	Sn–Bi–Sb alloys as anode materials for sodium ion batteries. Journal of Materials Chemistry A, 2017, 5, 9661-9670.	10.3	124

#	Article	IF	CITATIONS
55	Unrivaled combination of surface area and pore volume in micelle-templated carbon for supercapacitor energy storage. Journal of Materials Chemistry A, 2017, 5, 13511-13525.	10.3	63
56	Extremely high-rate aqueous supercapacitor fabricated using doped carbon nanoflakes with large surface area and mesopores at near-commercial mass loading. Nano Research, 2017, 10, 1767-1783.	10.4	103
57	Exceptional energy and new insight with a sodium–selenium battery based on a carbon nanosheet cathode and a pseudographite anode. Energy and Environmental Science, 2017, 10, 153-165.	30.8	184
58	Heteroatom enhanced sodium ion capacity and rate capability in a hydrogel derived carbon give record performance in a hybrid ion capacitor. Nano Energy, 2016, 23, 129-137.	16.0	170
59	Effects of washing and calcination–milling on ionic release and surface properties of yttria stabilized zirconia. Ceramics International, 2016, 42, 6755-6760.	4.8	4
60	Excellent energy–power characteristics from a hybrid sodium ion capacitor based on identical carbon nanosheets in both electrodes. Journal of Materials Chemistry A, 2016, 4, 5149-5158.	10.3	176
61	Tin and Tin Compounds for Sodium Ion Battery Anodes: Phase Transformations and Performance. Accounts of Chemical Research, 2015, 48, 1657-1665.	15.6	440
62	Pt–Au–Co Alloy Electrocatalysts Demonstrating Enhanced Activity and Durability toward the Oxygen Reduction Reaction. ACS Catalysis, 2015, 5, 1513-1524.	11.2	106
63	Sodiation vs. lithiation phase transformations in a high rate – high stability SnO ₂ in carbon nanocomposite. Journal of Materials Chemistry A, 2015, 3, 7100-7111.	10.3	100
64	Reactions in a multilayered Si (substrate)/Ta/Mg/Fe/Ta/Pd thin-film structure during annealing and deuterium absorption. Acta Materialia, 2015, 90, 259-271.	7.9	3
65	High rate SnO2–Graphene Dual Aerogel anodes and their kinetics of lithiation and sodiation. Nano Energy, 2015, 15, 369-378.	16.0	129
66	Coupling In Situ TEM and Ex Situ Analysis to Understand Heterogeneous Sodiation of Antimony. Nano Letters, 2015, 15, 6339-6348.	9.1	90
67	Sulfide promoted chronic fouling in a refinery: A broad phenomenon spanning a range of heat transfer surfaces and oil types. Fuel, 2015, 160, 479-489.	6.4	10
68	Titanium Oxynitride Interlayer to Influence Oxygen Reduction Reaction Activity and Corrosion Stability of Pt and Pt–Ni Alloy. ChemSusChem, 2015, 8, 361-376.	6.8	9
69	Peanut shell hybrid sodium ion capacitor with extreme energy–power rivals lithium ion capacitors. Energy and Environmental Science, 2015, 8, 941-955.	30.8	740
70	Thiophene mitigates high temperature fouling of metal surfaces in oil refining. Fuel, 2015, 139, 411-424.	6.4	15
71	Impregnation of La0.4Ce0.6O1.8–La0.4Sr0.6TiO3 as solid oxide fuel cell anode in H2S-containing fuels. Journal of Power Sources, 2015, 274, 211-218.	7.8	15
72	Tailoring Biomass-Derived Carbon Nanoarchitectures for High-Performance Supercapacitors. ChemElectroChem, 2014, 1, 302-302.	3.4	2

#	Article	IF	CITATIONS
73	Anodes for Sodium Ion Batteries Based on Tin–Germanium–Antimony Alloys. ACS Nano, 2014, 8, 4415-4429.	14.6	309
74	Lithium ion battery applications of molybdenum disulfide (MoS ₂) nanocomposites. Energy and Environmental Science, 2014, 7, 209-231.	30.8	1,172
75	Origin of non-SEI related coulombic efficiency loss in carbons tested against Na and Li. Journal of Materials Chemistry A, 2014, 2, 19685-19695.	10.3	179
76	Array geometry dictates electrochemical performance of Ge nanowire lithium ion battery anodes. Journal of Materials Chemistry A, 2014, 2, 16770-16785.	10.3	32
77	Si nanotubes ALD coated with TiO ₂ , TiN or Al ₂ O ₃ as high performance lithium ion battery anodes. Journal of Materials Chemistry A, 2014, 2, 2504-2516.	10.3	139
78	Activation with Li Enables Facile Sodium Storage in Germanium. Nano Letters, 2014, 14, 5873-5882.	9.1	116
79	Colossal pseudocapacitance in a high functionality–high surface area carbon anode doubles the energy of an asymmetric supercapacitor. Energy and Environmental Science, 2014, 7, 1708-1718.	30.8	381
80	Sulfur Refines MoO ₂ Distribution Enabling Improved Lithium Ion Battery Performance. Journal of Physical Chemistry C, 2014, 118, 18387-18396.	3.1	100
81	Nanometer-scale Sn coatings improve the performance of silicon nanowire LIB anodes. Journal of Materials Chemistry A, 2014, 2, 11261.	10.3	63
82	Hybrid Device Employing Three-Dimensional Arrays of MnO in Carbon Nanosheets Bridges Battery–Supercapacitor Divide. Nano Letters, 2014, 14, 1987-1994.	9.1	276
83	Tailoring Biomassâ€Đerived Carbon Nanoarchitectures for Highâ€Performance Supercapacitors. ChemElectroChem, 2014, 1, 332-337.	3.4	80
84	High-Density Sodium and Lithium Ion Battery Anodes from Banana Peels. ACS Nano, 2014, 8, 7115-7129.	14.6	779
85	Thermodynamically destabilized hydride formation in "bulk―Mg–AlTi multilayers for hydrogen storage. Physical Chemistry Chemical Physics, 2013, 15, 16432.	2.8	12
86	Nanocrystalline anatase TiO2: a new anode material for rechargeable sodium ion batteries. Chemical Communications, 2013, 49, 8973.	4.1	348
87	Effect of Asphaltene Stability on Fouling at Delayed Coking Process Furnace Conditions. Energy & Fuels, 2013, 27, 1856-1864.	5.1	13
88	Carbon Nanosheet Frameworks Derived from Peat Moss as High Performance Sodium Ion Battery Anodes. ACS Nano, 2013, 7, 11004-11015.	14.6	813
89	Silicon nanowire lithium-ion battery anodes with ALD deposited TiN coatings demonstrate a major improvement in cycling performance. Journal of Materials Chemistry A, 2013, 1, 12850.	10.3	114
90	ALD TiO2 coated silicon nanowires for lithium ion battery anodes with enhanced cycling stability and coulombic efficiency. Physical Chemistry Chemical Physics, 2013, 15, 13646.	2.8	156

#	Article	IF	CITATIONS
91	Mesoporous nitrogen-rich carbons derived from protein for ultra-high capacity battery anodes and supercapacitors. Energy and Environmental Science, 2013, 6, 871.	30.8	983
92	Supercapacitors based on carbons with tuned porosity derived from paper pulp mill sludge biowaste. Carbon, 2013, 57, 317-328.	10.3	155
93	Interconnected Carbon Nanosheets Derived from Hemp for Ultrafast Supercapacitors with High Energy. ACS Nano, 2013, 7, 5131-5141.	14.6	869
94	Magnesium and magnesium-silicide coated silicon nanowire composite anodes for lithium-ion batteries. Journal of Materials Chemistry A, 2013, 1, 1600-1612.	10.3	52
95	A TEM based study of the microstructure during room temperature and low temperature hydrogen storage cycling in MgH2 promoted by Nb–V. Acta Materialia, 2012, 60, 5646-5661.	7.9	52
96	Silicon nanowire core aluminum shell coaxial nanocomposites for lithium ion battery anodes grown with and without a TiN interlayer. Journal of Materials Chemistry, 2012, 22, 6655.	6.7	78
97	Highly corrosion resistant platinum–niobium oxide–carbon nanotube electrodes for the oxygen reduction in PEM fuel cells. Energy and Environmental Science, 2012, 5, 6156.	30.8	94
98	Graphene-nickel cobaltite nanocomposite asymmetrical supercapacitor with commercial level mass loading. Nano Research, 2012, 5, 605-617.	10.4	356
99	Cyclotron production of 99mTc: Recycling of enriched 100Mo metal targets. Applied Radiation and Isotopes, 2012, 70, 1685-1690.	1.5	46
100	Electrochemical Supercapacitor Electrodes from Sponge-like Graphene Nanoarchitectures with Ultrahigh Power Density. Journal of Physical Chemistry Letters, 2012, 3, 2928-2933.	4.6	173
101	TEM analysis of the microstructure in TiF3-catalyzed and pure MgH2 during the hydrogen storage cycling. Acta Materialia, 2012, 60, 6441-6456.	7.9	48
102	A knife-edge measurement of the beam profile of STXM 5.3.2.2 using a focussed ion beam milled metallic glass. Journal of Electron Spectroscopy and Related Phenomena, 2012, 185, 453-457.	1.7	4
103	Supercapacitive carbon nanotube-cobalt molybdate nanocomposites prepared via solvent-free microwave synthesis. RSC Advances, 2012, 2, 2753.	3.6	113
104	Stable Hydrogen Storage Cycling in Magnesium Hydride, in the Range of Room Temperature to 300 °C, Achieved Using a New Bimetallic Cr-V Nanoscale Catalyst. Journal of Physical Chemistry C, 2012, 116, 3188-3199.	3.1	54
105	Carbonized Chicken Eggshell Membranes with 3D Architectures as Highâ€₽erformance Electrode Materials for Supercapacitors. Advanced Energy Materials, 2012, 2, 431-437.	19.5	573
106	Carbonized Chicken Eggshell Membranes with 3D Architectures as High-Performance Electrode Materials for Supercapacitors (Adv. Energy Mater. 4/2012). Advanced Energy Materials, 2012, 2, 430-430.	19.5	10
107	Body centered cubic magnesium niobium hydride with facile room temperature absorption and four weight percent reversible capacity. Physical Chemistry Chemical Physics, 2012, 14, 10904.	2.8	38
108	Electrocatalytic hydrogenation of aromatic compounds in ionic liquid solutions over WS2-on-glassy carbon and Raney nickel cathodes. Fuel, 2012, 93, 415-422.	6.4	13

#	Article	IF	CITATIONS
109	Microstructural evolution during low temperature sorption cycling of Mg-AlTi multilayer nanocomposites. International Journal of Hydrogen Energy, 2012, 37, 4215-4226.	7.1	18
110	Effect of alloying magnesium with chromium and vanadium on hydrogenation kinetics studied with neutron reflectometry. Chemical Communications, 2011, 47, 4294.	4.1	23
111	High Rate Electrochemical Capacitors from Three-Dimensional Arrays of Vanadium Nitride Functionalized Carbon Nanotubes. Journal of Physical Chemistry C, 2011, 115, 24381-24393.	3.1	145
112	Corrosion-Fouling of 316 Stainless Steel and Pure Iron by Hot Oil. Energy & Fuels, 2011, 25, 4540-4551.	5.1	19
113	Deuterium absorption in Mg70Al30 thin films with bilayer catalysts: A comparative neutron reflectometry study. Journal of Alloys and Compounds, 2011, 509, 5466-5471.	5.5	5
114	Supercapacitive Properties of Hydrothermally Synthesized Co ₃ O ₄ Nanostructures. Journal of Physical Chemistry C, 2011, 115, 17599-17605.	3.1	179
115	Palladium Nanoparticles Formed on Titanium Silicate ETS-10. Journal of Nanoscience and Nanotechnology, 2011, 11, 2537-2539.	0.9	2
116	First principle study of hydrogen diffusion in equilibrium rutile, rutile with deformation twins and fluorite polymorph of Mg hydride. International Journal of Hydrogen Energy, 2011, 36, 11802-11809.	7.1	29
117	Microstructural evolution during hydrogen sorption cycling of Mg–FeTi nanolayered composites. Acta Materialia, 2011, 59, 2083-2095.	7.9	37
118	Hydrogen storage in bulk Mg–Ti and Mg–stainless steel multilayer composites synthesized via accumulative roll-bonding (ARB). International Journal of Hydrogen Energy, 2011, 36, 3022-3036.	7.1	64
119	Synergy of elemental Fe and Ti promoting low temperature hydrogen sorption cycling of magnesium. International Journal of Hydrogen Energy, 2011, 36, 6711-6722.	7.1	51
120	Design of high <i>T</i> _{<i>g</i>} Zr-based metallic glasses using atomistic simulation and experiment. Philosophical Magazine, 2011, 91, 3393-3405.	1.6	3
121	Oxygen Reduction Reaction Activity and Electrochemical Stability of Thin-Film Bilayer Systems of Platinum on Niobium Oxide. Journal of Physical Chemistry C, 2010, 114, 16463-16474.	3.1	55
122	Hydrogen storage in binary and ternary Mg-based alloys: A comprehensive experimental study. International Journal of Hydrogen Energy, 2010, 35, 2091-2103.	7.1	91
123	Early deuteration steps of Pd- and Ta/Pd- catalyzed Mg70Al30 thin films observed at room temperature. International Journal of Hydrogen Energy, 2010, 35, 10343-10348.	7.1	8
124	Analysis of deformation twins and the partially dehydrogenated microstructure in nanocrystalline magnesium hydride (MgH2) powder. Acta Materialia, 2010, 58, 3162-3172.	7.9	67
125	The role of self-shadowing on growth and scaling laws of faceted polycrystalline thin films. Acta Materialia, 2010, 58, 5150-5159.	7.9	11
126	Bimetallic Fe–V catalyzed magnesium films exhibiting rapid and cycleable hydrogenation at 200 °C. Applied Physics Letters, 2010, 96, .	3.3	24

#	Article	IF	CITATIONS
127	Hydrogen storage cycling of MgH2 thin film nanocomposites catalyzed by bimetallic Cr Ti. Applied Physics Letters, 2010, 97, .	3.3	54
128	Nanomechanical torque magnetometry of permalloy cantilevers. Journal of Applied Physics, 2010, 108, 123910.	2.5	9
129	Solid-state dewetting mechanisms of ultrathin Ni films revealed by combining <i>in situ</i> time resolved differential reflectometry monitoring and atomic force microscopy. Physical Review B, 2010, 82, .	3.2	31
130	Analytic description of competitive grain growth. Physical Review E, 2010, 81, 011601.	2.1	8
131	Nanosilver Particle Formation on a High Surface Area Titanate. Journal of Nanoscience and Nanotechnology, 2010, 10, 8448-8451.	0.9	4
132	Hydrogen Sorption Cycling Kinetic Stability and Microstructure of Single-Walled Carbon Nanotube (SWCNT) Magnesium Hydride (MgH ₂) Nanocomposites. Journal of Physical Chemistry C, 2010, 114, 3265-3275.	3.1	63
133	Electrocatalytic hydrogenation of 2-cyclohexen-1-one in a high sulfur environment using a carbon-supported nanostructured tungsten sulfide catalyst. Catalysis Communications, 2010, 12, 314-317.	3.3	10
134	Rapid and reversible hydrogen sorption in Mg–Fe–Ti thin films. Applied Physics Letters, 2009, 95, 103114.	3.3	49
135	Low temperature hydrogen desorption in MgAl thin films achieved by using a nanoscale Ta/Pd bilayer catalyst. Applied Physics Letters, 2009, 94, 241901.	3.3	23
136	The influence of SWCNT–metallic nanoparticle mixtures on the desorption properties of milled MgH ₂ powders. Nanotechnology, 2009, 20, 204016.	2.6	60
137	Structural changes of thin MgAl films during hydrogen desorption. Nuclear Instruments and Methods in Physics Research, Section A: Accelerators, Spectrometers, Detectors and Associated Equipment, 2009, 600, 301-304.	1.6	11
138	Nano-scale bi-layer Pd/Ta, Pd/Nb, Pd/Ti and Pd/Fe catalysts for hydrogen sorption in magnesium thin films. International Journal of Hydrogen Energy, 2009, 34, 7741-7748.	7.1	54
139	Simulations of faceted polycrystalline thin films: Asymptotic analysis. Acta Materialia, 2009, 57, 1327-1336.	7.9	15
140	TEM analysis and sorption properties of high-energy milled MgH2 powders. Journal of Alloys and Compounds, 2009, 476, 590-598.	5.5	54
141	Neutron reflectometry study of hydrogen desorption in destabilized MgAl alloy thin films. Applied Physics Letters, 2008, 92, 121917.	3.3	35
142	The synthesis of a platy chabazite analog from delaminated metakaolin with the ability to surface template nanosilver particulates. Clays and Clay Minerals, 2008, 56, 655-659.	1.3	4
143	Metal nanodots formed and supported on chabazite and chabazite-like surfaces. Microporous and Mesoporous Materials, 2007, 103, 309-315.	4.4	24
144	Metallic NEMS components fabricated from nanocomposite Al–Mo films. Nanotechnology, 2006, 17, 3063-3070.	2.6	223

#	Article	IF	CITATIONS
145	Structure–properties relations in spot friction welded (also known as friction stir spot welded) 6111 aluminum. Materials Science & Engineering A: Structural Materials: Properties, Microstructure and Processing, 2006, 441, 79-96.	5.6	133
146	Strain-compensated nano-clusters in Al–Si–Ge alloys. Scripta Materialia, 2006, 54, 1973-1978.	5.2	7
147	Formation of nanoporous noble metal thin films by electrochemical dealloying of PtxSi1â^'x. Applied Physics Letters, 2006, 88, 033110.	3.3	131
148	Role of Strain-Compensated Clusters in Al-Alloy Design. , 2006, , .		0
149	Impact of heat on nanocrystalline silver dressings. Biomaterials, 2005, 26, 7230-7240.	11.4	48
150	Formation of misfit dislocations in nanoscale Ni–Cu bilayer films. Philosophical Magazine, 2004, 84, 719-736.	1.6	48
151	On the influence of Siâ^'Ge additions on the aging response of Alâ^'Cu. Metallurgical and Materials Transactions A: Physical Metallurgy and Materials Science, 2003, 34, 735-742.	2.2	10